Aero-Propulsive Efficiency Requirements for Turboelectric Transport Aircraft

de Vries, Reynard; Hoogreef, Maurice; Vos, Roelof

DOI
10.2514/6.2020-0502

Publication date
2020

Document Version
Final published version

Published in
AIAA Scitech 2020 Forum

AIAA SciTech Forum
6-10 January 2020, Orlando, FL
AIAA Scitech 2020 Forum

10.2514/6.2020-0502

Aeropropulsive Efficiency Requirements for Turboelectric Transport Aircraft

Reynard de Vries*, Maurice F. M. Hoogreef† and Roelof Vos‡
Delft University of Technology, Kluyverweg 1, 2629HS Delft, The Netherlands

In this paper a design-of-experiments is performed with the objective of determining the improvements in aeropropulsive efficiency required for a reduction in the energy consumption of turboelectric transport aircraft, when compared to conventional, gas-turbine based alternatives. Simplified representations of the powertrain and the aeropropulsive interaction effects are used, such that the results are independent of the design of the electrical system or the external layout of the propulsion-system. An evaluation of different mission requirements confirms that the turboelectric architecture presents the largest benefit for long ranges, and that the aeropropulsive benefit required for a predefined reduction in energy consumption increases with increasing cruise Mach number. Moreover, the impact of different technology maturity levels of the electrical drivetrain components is assessed. The results show that the shaft power ratio necessary to achieve a determined aeropropulsive benefit is a decisive factor, and that for a shaft power ratio of 20%, a 5% reduction in energy consumption is possible on the mid-term (circa 2035) if an 11% increase in aeropropulsive efficiency is achieved. A 15% reduction in energy consumption is only possible with extremely optimistic powertrain technology assumptions, and requires and increase in aeropropulsive efficiency of at least 14%, for the missions considered.

Nomenclature

Symbols

A	=	Aspect ratio [-]
a	=	Speed of sound [m/s]
C_D	=	Drag coefficient, $D/(0.5\rho V^2 S)$ [-]
C_{D0}	=	Zero-lift drag coefficient [-]
C_L	=	Lift coefficient, $L/(0.5\rho V^2 S)$ [-]
$C_{L\max}$	=	Maximum lift coefficient [-]
D	=	Drag [N]
e	=	Oswald factor [-]
g	=	Gravitational acceleration [m/s^2]
h	=	Altitude [m]
L	=	Lift [N]
M	=	Mach number, V/a [-]
m	=	Mass [kg]
P	=	Power [W]
R	=	Range [m]
S	=	Wing area [m^2]
T	=	Thrust [N]
V	=	Velocity [m/s]
W	=	Weight, $m \cdot g$ [N]
$\Delta(\ )$	=	Difference between HEP and reference aircraft
η	=	Efficiency [-]
ρ	=	Freestream density [kg/m^3]
φ	=	Shaft power ratio [-]

Abbreviations

CSP	=	Combined specific power [kW/kg]
DoE	=	Design of experiments
EM	=	Electrical machine
F	=	Fuel
GB	=	Gearbox
GT	=	Gas turbine
HEP	=	Hybrid-electric propulsion
MTOM	=	Maximum take-off mass [kg]
P	=	Propulsor
PM	=	Power management and distribution system
PREE	=	Payload-range energy efficiency [-]
SP	=	Specific power [kW/kg]

Additional subscripts

chain	=	Chain (efficiency)
L	=	Landing
miss	=	Nominal mission (excl. reserves)
opt	=	Optimum
PL	=	Payload
p	=	Propulsive
ref	=	Reference (fuel-based) aircraft
s	=	Shaft
TO	=	Take-off
1	=	Primary powertrain branch
2	=	Secondary powertrain branch

*PhD Candidate, Faculty of Aerospace Engineering, R.deVries@tudelft.nl, AIAA member.
†Assistant Professor, Faculty of Aerospace Engineering, M.F.M.Hoogreef@tudelft.nl, AIAA Member
‡Assistant Professor, Faculty of Aerospace Engineering, R.Vos@tudelft.nl, AIAA Associate Fellow.

I. Introduction

Numerous studies on hybrid-electric propulsion have been performed in recent years, with the goal of reducing emissions [1–3], reducing operating costs [4], or enabling new missions for which aircraft were traditionally not competitive [5]. A large fraction of these studies focuses on regional [6–10] and short- or long-haul [11–19] commercial transport aircraft, since these markets constitute the dominant contribution to the environmental impact of aviation [20], and a radical change in the design of these aircraft is required in order to meet the long-term sustainability goals established by the European Commission [21] and NASA [22]. However, multiple studies have already shown that this step-change is a difficult task for large passenger aircraft, even when assuming appreciable advances in electrical-component technology with respect to the current state-of-the-art [9, 14, 15].

In this paper, "hybrid-electric propulsion" (HEP) is defined as the use of electrical energy in the generation or transmission of the power used for propulsion. It therefore includes a spectrum of powertrain architectures, with a conventional combustion-based powertrain at one end of the spectrum, and a fully-electric powertrain at the other end. Serial, parallel, or turboelectric architectures are therefore considered subsets of HEP (see e.g. Refs. [23, 24]), contrary to some other classifications which make a distinction between hybrid-electric (electrical and non-electrical energy storage) and turboelectric (only non-electrical energy storage) propulsion [25]. When analyzing the existing literature, it becomes evident that, for large passenger aircraft, hybrid-electric propulsion can be used in two ways to improve aircraft efficiency. The first aims to improve the powertrain efficiency, i.e., to improve the efficiency of the gas turbine or the transmission efficiency from the energy sources to the shaft of the propulsive device. The second aims to improve the *aeropropulsive* efficiency of the aircraft, i.e., to increase the lift-to-drag ratio of the aircraft or the thrust-to-power ratio of the propulsive devices. Although both options are enabled by hybrid-electric propulsion, they represent very distinct design strategies. The former requires the use of batteries, and is typically applied in a parallel powertrain architecture (see e.g. Refs. [19, 26–29]), without significant modifications to the airframe. The latter does not necessarily use batteries, but takes advantage of the scalability of electrical machines and the versatility of electrical power distribution to place the propulsive devices at beneficial locations on the airframe. This leads to noticeable changes in the external layout of the aircraft and, based on previous studies, presents the largest benefit when used in a (partial-) turboelectric configuration [9, 15].

The study presented in this paper focuses on the second application, that is, on the use of HEP to increase the aeropropulsive efficiency of the aircraft. There are two reasons for this. Firstly, because the long-term environmental impact of aviation cannot be reduced effectively without significant improvements in the aerodynamic and propulsive efficiency of the aircraft. And secondly because, even though several turboelectric aircraft design studies have been performed [13, 18, 30, 31], there is still a large uncertainty regarding the benefits of such aircraft, especially due to the lack of propulsion-airframe integration studies. While the aerodynamic benefits of novel propulsion-system layouts such as leading-edge distributed propulsion [32], over-the-wing propulsion [33], under-the-wing propulsion [13], boundary-layer ingestion [34], or tip-mounted propulsion [35] have been studied at subsystem level, it is still unclear which of these configurations leads to the greatest benefit at aircraft level. Although such propulsion systems do not necessarily need a hybrid-electric powertrain [36], many radical aircraft configurations with improved propulsion–airframe integration are only viable when combined with HEP, and thus the overall benefit is highly dependent on the maturity of the powertrain components [37].

The goal of this paper is therefore to estimate the aeropropulsive benefit required in order to make a turboelectric transport aircraft more efficient than a conventional turboprop or turbofan aircraft. To this end, a reverse-engineering approach is taken: assume there is a turboelectric aircraft which, by some means of propulsion, gives an aeropropulsive benefit. To obtain this benefit, electrical components of a determined technology level (i.e. specific power and transmission efficiency) are required. In that case, what are the technology-level requirements for an X% reduction in energy consumption, when compared to a conventional aircraft configuration? For which mission are these technology requirements the lowest, i.e., for which mission will the turboelectric aircraft be competitive the "soonest"? To answer these questions, the preliminary sizing of a turboelectric passenger aircraft is performed for different input parameters in a design-of-experiments (DoE), and the resulting energy consumption is computed. Section II describes the approach taken for this design-of-experiments, and shows how the results are kept independent of the type of propulsion system employed. Subsequently, Sec. III presents the estimated aeropropulsive efficiency requirements for different mission parameters, technology levels, and overall energy-reduction levels. The obtained values provide, within the uncertainty of a Class-I sizing method, a means for designers to relate the findings of aerodynamic studies to their impact on energy consumption, or, from the reverse-engineering perspective, to determine which component technology levels are required for a specific propulsion-system layout to be beneficial.

II. Approach

This section describes the methodology followed in order to estimate the aeropropulsive requirements for a generic turboelectric transport aircraft. A simplified representation of the turboelectric powertrain is described in Sec. II.A. Section II.B then defines the aeropropulsive efficiency, and discusses how this efficiency can be related to the individual aerodynamic characteristics of the aircraft, and what impact this has on the sizing process. Finally, Sec. II.C describes the design-of-experiments performed in order to obtain a response surface for the selected figure of merit.

A. Powertrain Architecture Definition

A turboelectric powertrain consists of a gas turbine—or any other combustion engine or device which converts a consumable energy source into mechanical power—connected to a generator that transforms the mechanical power into electrical power, which is then distributed to one or more electrical motors that drive the propulsive devices. In this study, a more elaborate variant, known as the *partial-turboelectric* architecture [24], is considered. A simplified schematic representation of this architecture is depicted in Fig. 1, which differs from a fully-turboelectric architecture due to the presence of a propulsor which is mechanically driven by the gas turbine (P1). The gas turbine therefore exhibits a power off-take (e.g., a separate low-pressure turbine stage or a gearbox) which drives an electrical machine (EM1). Therefore, the powertrain contains a node where the power is split into two paths, indicated by a gearbox (GB) in Fig. 1. The extracted electrical power is then routed through a power management and distribution system (PM), and finally absorbed by secondary electrical machines (EM2), which drive a second set of propulsors.

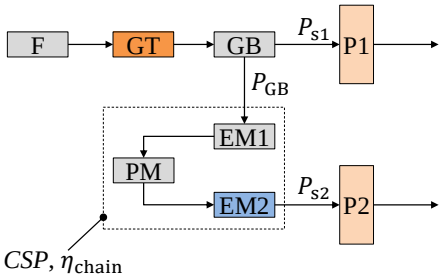

Fig. 1 Notional representation of the partial-turboelectric powertrain architecture, indicating component nomenclature.

The powertrain description is further simplified by grouping all electrical components into a single "black box" which represents the electrical drivetrain and is characterized by two parameters, namely a *chain efficiency*, η_{chain}, and a *combined specific power* (CSP). The former is defined as the ratio between the output power and input power of the electrical drivetrain, that is, it represents the combined transmission efficiency of all components:

$$\eta_{\text{chain}} = \frac{P_{s2}}{P_{GB}} = \prod_{i=1}^{k} \eta_i, \tag{1}$$

where the index i covers all the k electrical components connected in series, each of which presents a determined transmission efficiency η_i. The combined specific power, meanwhile, is defined as the power introduced to the electrical drivetrain divided by the total mass of all components in said drivetrain, and is typically expressed in kW/kg:

$$\text{CSP} = \frac{P_{GB}}{\sum_{i=1}^{n} m_i}, \tag{2}$$

where m is the mass of each component in the electrical drivetrain and n the number of components. If the losses in the drivetrain are small ($\eta_{\text{chain}} \approx 1$), then the combined specific power can be computed based on the specific power (SP) of each component as:

$$\text{CSP} \approx \sum_{i=1}^{n} \frac{1}{(1/\text{SP}_i)}. \tag{3}$$

Although the "black box" simplification makes this approach unsuitable for detailed studies, it has several advantages. Firstly, it provides a more simplified, top-level understanding of the effect of powertrain technology levels, since it does

not require information regarding every component in the powertrain. Secondly, the number of dimensions of the DoE is significantly reduced, given that the electrical drivetrain is now parametrized by just two variables. Thirdly, the findings of this study are therefore independent of the design of the electrical system (AC vs. DC transmission, active vs. passive cooling, redundant wiring, etcetera). The relation between the individual properties of each component and the global properties, CSP and η_{chain}, can be established ad-hoc on a case-to-case basis. As an example, Table 1 presents the chain efficiency and CSP computed for the three hypothetical technology scenarios discussed in Sec. III.C. The mid-term scenario corresponds to the research goals listed in Ref. [11]. For this table, the electrical drivetrain of the powertrain is assumed to be comprised of two sets of electrical machines (generators and motors) and two sets of power converters (rectifiers and inverters), to which an additional 30% weight penalty is added to account for additional elements of the power distribution and thermal management system. Although in this study an arbitrary 30% penalty is assumed, in practice the designer would have to perform a more accurate estimation of the electrical components' weights, and compute the CSP and chain efficiency based on the outcome.

Table 1 CSP and chain efficiency of three hypothetical technology scenarios.

Scenario	**Electrical machines**		**Power converters**		**PMAD/cooling**		**Complete chain**	
	SP [kW/kg]	η [-]	SP [kW/kg]	η [-]	weight penalty		CSP [kW/kg]	η_{chain} [-]
Near-term	9	0.92	13	0.97	30%	→	2	0.80
Mid-term	13	0.96	19	0.99	30%	→	3	0.90
Long-term	22	0.99	32	1.00	30%	→	5	0.98

A third parameter is required to characterize the power share between the primary and secondary propulsion system. This variable is the *shaft power ratio*, defined as

$$\varphi = \frac{P_{s2}}{P_{s1} + P_{s2}}. \tag{4}$$

The power flow across the powertrain can be computed based on φ for a given throttle setting or propulsive-power requirement following the matrix formulation of Ref. [23]. This power-control parameter has to be chosen by the designer for each flight condition. In this study, for simplicity, a constant shaft power ratio is assumed for all performance constraints and mission segments. A value of $\varphi = 0$ therefore corresponds to a conventional, fuel-based architecture, while $\varphi = 1$ corresponds to a fully-turboelectric architecture. Although previous studies have shown that a fully turboelectric architecture is unlikely to provide any benefits in the near term due to the increased weight of electrical components [9, 15], it is included as a limit case in this study. It is evident that for $\varphi = 0$ the power transmitted by—and thus the weight of—the electrical components is zero, and therefore the conventional powertrain is the lightest. However, per definition this limit case also corresponds to zero aeropropulsive benefit, since there is no enhanced propulsion–airframe integration. This trade-off between the aeropropulsive benefit achievable for a given shaft power ratio and the associated weight penalty is assessed in Sec. III.

B. Aeropropulsive Efficiency Breakdown

Figure 2 presents a series of propulsion-system layouts which are compatible with the powertrain architecture described in the previous section. Each notional example has two gas turbines driving an open rotor or ducted fan, as well as a secondary propulsion system comprising one or more electrically-driven fans or propellers. In all cases, the secondary system enhances the aerodynamic and/or propulsive performance of the aircraft. For example, the tip-mounted propulsors decrease the lift-induced drag of the wing, effectively increasing the equivalent aspect ratio or span efficiency of the wing [35]. The leading-edge propellers can increase the maximum lift coefficient of the wing [32], leading to a significant increase in wing loading [23, 38]. Over-the-wing propulsion, meanwhile, increases the lift-to-drag ratio of the wing [33]. Finally, the use of boundary-layer ingestion affects airframe drag and increases the thrust-to-power ratio of the rear propulsor [34, 39], which, from a preliminary sizing perspective, can be modeled as an change in propulsive efficiency and drag coefficient. Finally, for a given primary-propulsor size, the addition of extra propulsors increases the total disk area, leading to a decrease in disk loading (or fan pressure ratio) and a consequent increase in propulsive efficiency [18].

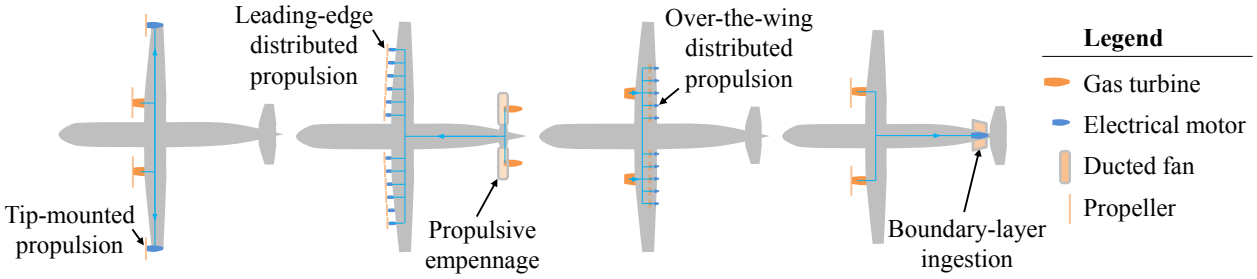

Fig. 2 Examples of (partial-) turboelectric aircraft configurations.

1. Factors Affecting the Aeropropulsive Efficiency

The examples provided in Fig. 2 illustrate how distributed propulsion can enhance the aeropropulsive performance of the aircraft in multiple ways. In order to assess the impact of this performance benefit at aircraft level, the propulsive efficiency is multiplied by the aerodynamic efficiency (lift-to-drag ratio) to define an overall *aeropropulsive efficiency* as

$$\eta_\mathrm{p} \cdot \frac{L}{D} = \eta_\mathrm{p} \left(\frac{C_L}{C_{D0} + \dfrac{C_L^2}{\pi A e}} \right), \tag{5}$$

where a symmetric parabolic lift polar is assumed for simplicity. This overall aeropropulsive efficiency differs from the commonly used range parameter [40] because η_p refers exclusively to the propulsive efficiency of the propellers or fans, that is,

$$\eta_\mathrm{p} = \frac{TV}{P_\mathrm{s}} = (1-\varphi)\eta_{\mathrm{p}1} + \varphi\eta_{\mathrm{p}2}, \tag{6}$$

where $\eta_{\mathrm{p}1}$ and $\eta_{\mathrm{p}2}$ are the propulsive efficiencies of the primary (P1) and secondary (P2) propulsors, respectively, and $P_\mathrm{s} = P_{\mathrm{s}1} + P_{\mathrm{s}2}$ is the total shaft power.

Equation 5 indicates four direct ways in which distributed propulsion can be used to enhance the aeropropulsive performance of the aircraft: by decreasing the zero-lift drag coefficient, reducing the lift induced drag (through an equivalent increase in aspect ratio or Oswald factor), increasing the propulsive efficiency, or by changing the lift coefficient. The lift coefficient varies throughout the mission, and depends on the flight condition (speed and altitude) and wing loading—which, in turn, depends on the maximum lift coefficient. In this study, the effect of improved propulsion–airframe integration is simulated by varying the aeropropulsive efficiency as a whole. This simplifies the problem and leads to conclusions which are independent of the type of propulsion system, analogously to the simplification made in Sec. II.A regarding the powertrain parametrization. The change in aeropropulsive efficiency can then be related to the effect of a determined propulsion system on a case-to-case basis.

The sensitivity of the aeropropulsive efficiency to variations in the individual aerodynamic characteristics can be estimated with reasonable accuracy using Eq. 5, as demonstrated in Fig. 3a-3d. These figures present the percentage change in aeropropulsive efficiency versus a percentage change in each of the aerodynamic characteristics. The figures compare the value predicted by Eq. 5 with the mission-averaged value obtained from a complete Class-I sizing process of a generic transport aircraft, including climb, descent, and diversion phases. Although theoretically the impact of Oswald factor and aspect ratio on the aeropropulsive efficiency are the same, they have been included separately since the aspect ratio also affects the wing weight. Furthermore, even though Fig. 3 shows that the aeropropulsive efficiency is most sensitive (and directly proportional) to η_p, it is important to note that η_p cannot exceed unity, and therefore a percent increase in propulsive efficiency may be much more difficult to achieve in practice than, for example, a percentage increase in aspect ratio.

The link between $C_{L\max}$ and the aeropropulsive efficiency (Fig. 3e) can be established once the operating conditions, drag polar, and wing loading of the specific aircraft configuration are known. Establishing a generic relation between the maximum lift coefficient and the aeropropulsive efficiency, on the other hand, is more complicated, as discussed in Sec. II.B.2. This is especially the case because the maximum lift coefficient is closely coupled to the optimum cruise altitude, and previous work has already highlighted the importance of evaluating HEP aircraft at optimum cruise

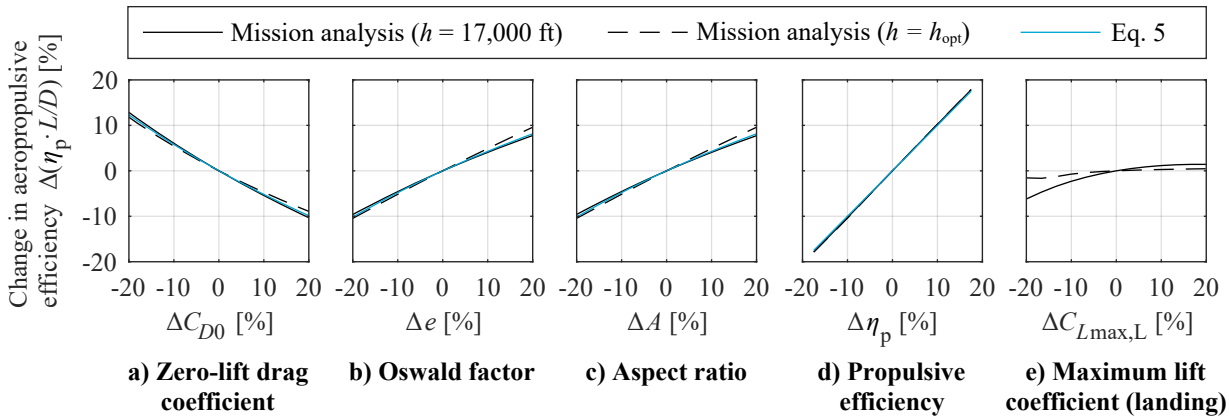

Fig. 3 Example of the impact of individual aerodynamic characteristics on the overall aeropropulsive efficiency of a generic turboelectric aircraft, comparing Eq. 5 with results obtained from mission analyses at fixed cruise altitude and optimum cruise altitude.

altitude when assessing the impact of distributed propulsion [9]. To illustrate this dependency, Fig. 3 includes both the aeropropulsive efficiency obtained at constant altitude, and the one obtained if the cruise altitude is tailored to minimize energy consumption. Although this does not have a large effect on the sensitivities presented in subplots a–d, it does have a large impact on the sensitivity to maximum lift coefficient: if the maximum lift coefficient varies, the optimum cruise altitude changes, but the aeropropulsive efficiency remains nearly constant. These trends show how e.g. leading-edge distributed propulsion does not necessarily have a beneficial impact on the aerodynamic efficiency of the aircraft if the aspect ratio is maintained*. For more information on this topic, the reader is referred to the work of the X-57 demonstrator [32, 38].

2. Impact on Aircraft Sizing Process

The influence of variations in aeropropulsive efficiency can be observed in two steps of the sizing process: in the performance constraint analysis (power requirements), and in the mission analysis (energy requirements). The impact on power requirements can be visualized in the constraint diagram, a notional example of which is given in Fig. 4. In this diagram, only the take-off distance, cruise speed, and stall speed constraints are included for simplicity. The figure shows how a decrease in drag coefficient or an increase in propulsive efficiency displaces the take-off and cruise constraints upwards, expanding the feasible design space and enabling higher power-loading values. This leads to a smaller powertrain (per unit weight of the aircraft), thereby reducing the powertrain weight fraction and, consequently, the aircraft weight. The maximum lift coefficient, meanwhile, has a more pronounced effect, since it also determines the stall speed constraint. An increase in $C_{L\max}$ leads to a smaller wing (per unit weight of the aircraft), which affects the wing weight fraction as well as the lift coefficient throughout the entire mission. This in turn decreases the optimum cruise altitude of the aircraft or, for a given cruise altitude, increases or decreases the cruise lift-to-drag ratio, depending on the cruise speed and the characteristics of the drag polar. Moreover, the power loading of the aircraft is also affected, since the stall speed constraint intersects the power-limiting constraint at a different location in the diagram. The power loading can increase or decrease, depending on the trend of the limiting constraint. These dependencies illustrate how the effect of the maximum lift coefficient on the aircraft's design is much less trivial than the effect of, for example, the zero-lift drag coefficient or propulsive efficiency.

The aeropropulsive efficiency also plays an important role when computing the energy requirements of the aircraft. As is the case for conventional fuel-based aircraft, in most hybrid-electric aircraft design studies, the energy required to complete a predefined mission is estimated by integrating the energy consumption along a time-stepping simulation of the mission profile (see e.g. Refs. [2, 8, 23]). In quasi-level, quasi-steady flight, the required shaft power can be expressed as

$$P_s = \frac{W \cdot V}{\eta_p (L/D)}, \tag{7}$$

*Note that the increased wing-loading enabled by distributed propulsion also has other benefits, such as improved take-off and landing capabilities, a reduced optimum cruise altitude, or an increased maximum allowable aspect ratio for a given span constraint.

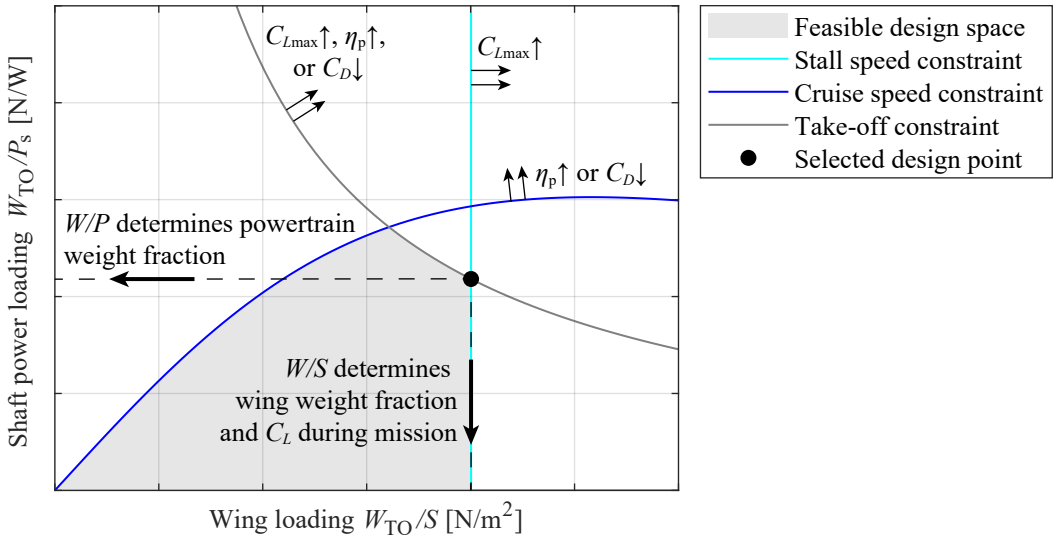

Fig. 4 Notional wing-loading–power-loading diagram, indicating how the aeropropulsive characteristics of the aircraft affect its performance constraints.

which indicates that the energy consumed in each differential time step is inversely proportional to the aeropropulsive efficiency[†]. Because of this, the effect of an increase in aeropropulsive efficiency on the overall energy consumption of commercial transport aircraft is determined primarily in the mission analysis (sizing for energy), and not so much in the constraint diagram (sizing for power). For example, for a generic turboelectric aircraft considered in this study (R = 825 nmi, M = 0.41, m_{PL} = 7500 kg, φ = 0.5), a 10% increase in aeropropulsive efficiency in only the mission analysis leads to a 12% reduction in energy consumption, while a 10% increase in aeropropulsive efficiency in only the constraint diagram leads to just a 1% reduction in energy consumption. For longer ranges, this difference is more pronounced. For aircraft with small fuel weight fractions and high powertrain weight fractions, on the other hand, variations in aeropropulsive efficiency can have a more dominant impact on the power-loading diagram, and less impact on the energy requirements computed in the mission analysis.

C. Design of Experiments

The modified Class-I sizing routine described in Ref. [23] is used to size the turboelectric aircraft for a range of input parameters. This method has been validated by comparing the results to an independently-developed HEP sizing routine in Ref. [41]. The baseline requirements, design parameters, and assumptions can be found in Ref. [9]. The input parameters that are varied in the DoE are gathered in Table 2. Although the baseline reference aircraft is based on a regional turboprop, the mission parameters (harmonic range, payload mass and cruise Mach number) are also sampled at higher values to analyze the trends in the regional jet or short-haul market, comparable to recent research on high-capacity turboprop aircraft [42]. A payload mass of 100 kg is assumed per passenger, including luggage. A conventional, fuel-based reference aircraft is also sampled for the same range of mission requirements, in order to compare the performance of the HEP variant to a conventional aircraft sized for the same mission. In both cases, the optimum cruise altitude in terms of minimum energy consumption is computed and subsequently selected for each point.

In addition to the mission requirements, the powertrain technology level is varied by modifying the combined specific power and chain efficiency of the powertrain. This is done by scaling the specific power and transmission efficiency of all electrical components included in the sizing method equally, such that the desired CSP and η_{chain} are obtained. Furthermore, the shaft power ratio of the aircraft is varied, applying the same value to all mission segments and performance constraints. Finally, the impact of HEP on the aeropropulsive performance of the aircraft is simulated by scaling the zero-lift drag and lift-induced drag components equally. Two main output parameters are monitored: the maximum take-off mass (MTOM) of the aircraft, and the payload-range energy efficiency (PREE). The latter is used as

[†]This is true for a given aircraft weight; in the sizing process, the energy consumption is actually more sensitive to the aeropropulsive efficiency due to the cyclic "snowball" effect.

Table 2 List of input parameters varied in the DoE, including the range of values sampled.

Parameter	Minimum	Maximum
M	0.45	0.65
m_{PL} [t]	5 (50 pax)	20 (200 pax)
R [nmi]	500	2000
CSP [kW/kg]	1.5	6
η_{chain}	0.8	1.0
φ	0	1
$\Delta(\eta_{\mathrm{p}} L/D)$	-50%	+50%

figure-of-merit in this study. This non-dimensional parameter represents the overall energy efficiency of the aircraft, being inversely proportional to the amount of energy consumed for a given mission requirement [9, 36]:

$$\mathrm{PREE} = \frac{W_{\mathrm{PL}} R}{E_{\mathrm{miss}}}. \tag{8}$$

Note that this definition of PREE only considers the energy consumed during the nominal mission, E_{miss}, and not the reserves. In this way, the parameter is representative of the energy consumed in the day-to-day operation of the aircraft.

A Latin-hypercube sampling of 20,000 points is performed for the input parameters given in Table 2, and the sizing routine is applied successively. In order to obtain continuous gradients in the results, a seven-dimensional, 7$^{\mathrm{th}}$ order polynomial fit is applied using a linear-least-squares algorithm. Of the 20,000 points, 95% are used to generate the surrogate model, while the remaining 5% are used to evaluate the accuracy of the fit and to ensure that no over-fitting occurs. Results are only analyzed in the intervals given in Table 2, i.e., no extrapolation is performed. The mean deviation of the surrogate model from the data points is found to be below 0.01%, with a maximum deviation of 0.8% for MTOM, and 0.3% for PREE. Therefore, although these values lie well within the accuracy of a Class-I sizing routine, an additional uncertainty of approximately ±1% should be kept in mind when analyzing the results.

III. Aeropropulsive Efficiency Requirements for Improved Aircraft Efficiency

The results are grouped into two sections. First, Sec. III.A describes how the aeropropulsive requirements depend on the mission parameters. Section III.B then describes how these requirements evolve with the powertrain technology level. Finally, Sec. III.C presents a summary of the results and discusses the relevance and implications of the findings.

A. Impact of Mission Requirements

Figure 5 presents the payload-range energy efficiency of the reference (fuel-based) aircraft and the turboelectric variant, as a function of the mission payload and range. For the turboelectric aircraft, a 10% increase in aeropropulsive efficiency (i.e., $(\eta_{\mathrm{p}} L/D)_{\mathrm{HEP}}/(\eta_{\mathrm{p}} L/D)_{\mathrm{ref}} = 1.1$) has been assumed, together with a shaft power ratio of $\varphi = 0.2$. The maps show that both the conventional and the turboelectric aircraft are most efficient at a range of approximately 650 nmi, with a payload of 20 t (Point A). Although the trends of the two aircraft are the same, the turboelectric variant presents a slightly higher PREE for the technology scenario and aeropropulsive benefit considered.

In order to further analyze the difference between the turboelectric and the conventional aircraft, Fig. 6 presents the aeropropulsive efficiency gain necessary for a 15% increase in PREE, that is, for a 15% energy reduction with respect to the reference aircraft on the same mission. The results are displayed for a generic value of $\Delta\mathrm{PREE} = 15\%$ because, from a commercial perspective, a significant energy saving is required to outweigh the additional complexity and development costs of such aircraft. Figure 6 shows that a significant increase in aeropropulsive efficiency of around 20% is required for a 15% energy reduction. The percentage change in aeropropulsive efficiency is larger than the percentage reduction in energy consumption, because the additional weight and efficiency losses of the hybrid-electric powertrain must be compensated. The required aeropropulsive benefit is practically independent of the payload considered, and decreases with increasing range. This occurs because, for longer ranges, the amount of fuel saved increases. This leads to a direct energy saving on one hand, and decreases the weight penalty of the turboelectric aircraft on the other, since the fuel weight increases less with range for the turboelectric aircraft than for the conventional one. Therefore, while point A represents the combination of payload and range where the turboelectric aircraft is most efficient (within the m_{PL} and R

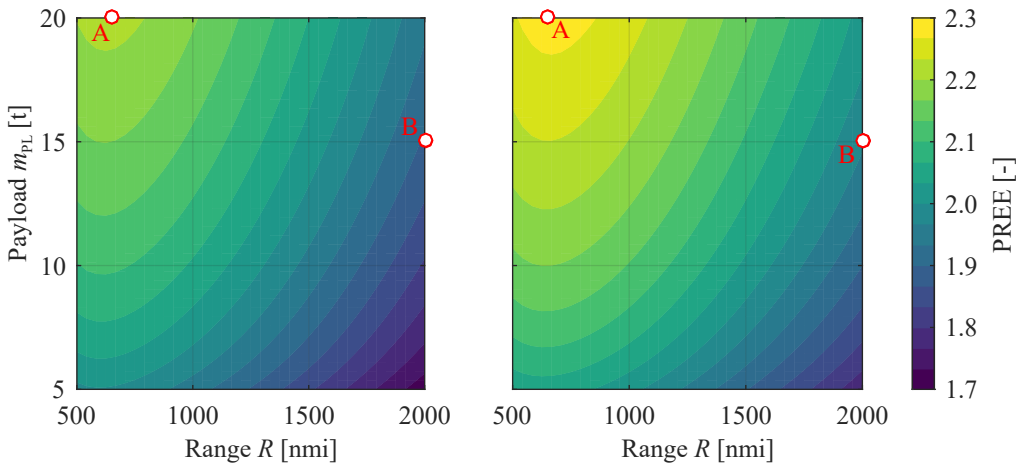

Fig. 5 Payload-range energy efficiency as a function of mission requirements for the reference (left) and partial turboelectric (right) aircraft, assuming a 10% increase in aeropropulsive efficiency for the latter (M = 0.55, η_{chain} = 0.9, CSP = 3 kW/kg, φ = 0.2). Markers indicate the mission scenarios collected in Tables 3 and 4.

intervals studied), point B—or any other point for R = 2000 nmi—represents the mission for which the turboelectric presents the greatest benefit when compared to the reference aircraft. This confirms that turboelectric configurations are most competitive for longer ranges, which is why many turboelectric aircraft design studies focus on medium- and long-haul flights [13, 18, 30], and not on the regional or thin-haul market. This also highlights an important difference compared to other hybrid-electric aircraft that make use of batteries, for which the extra battery weight generally implies that reduced ranges have to be flown (see e.g. Refs. [2, 4, 6, 29]).

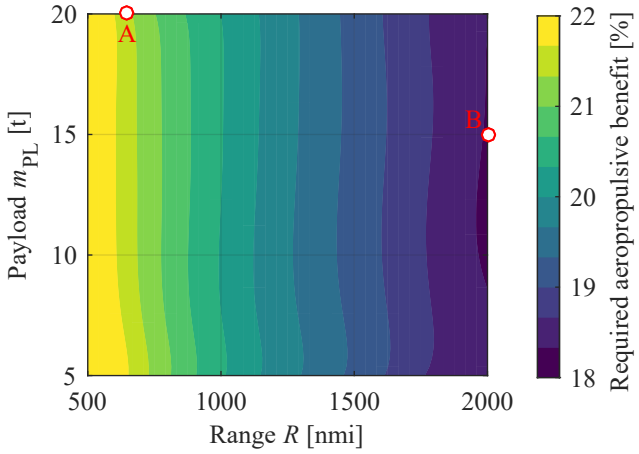

Fig. 6 Aeropropulsive efficiency increase required in order to obtain a 15% increase in PREE, as a function of mission range and payload (M = 0.55, η_{chain} = 0.9, CSP = 3 kW/kg, φ = 0.2). Markers indicate the mission scenarios collected in Tables 3 and 4.

Finally, the effect of cruise Mach number is assessed in Fig. 7. This figure presents the same variables as Fig. 6, but at a constant payload of 15t (150 pax) and for three different Mach numbers. Again, the figure clearly shows that a 15% energy reduction is most easily achieved at long ranges. Furthermore, the required aeropropulsive efficiency benefit increases with Mach number. In other words, a determined energy saving is easier to achieve with a low-speed turboelectric aircraft than with a high-speed one. This occurs because, at high Mach numbers, the power required during cruise increases, and hence the cruise-speed constraint descends in the loading diagram (see Fig. 4). Given that, for the

range of Mach numbers considered, the cruise-speed constraint is actively sizing the powertrain, this translates into a reduced power loading. Moreover, since the turboelectric powertrain is heavier than a gas turbine alone, the powertrain weight fraction increases much faster with Mach number for the turboelectric aircraft than for the reference aircraft. This leads to a larger difference in MTOM between the two configurations, and consequently, the turboelectric aircraft requires an additional aeropropulsive benefit to offset this weight increase at higher Mach numbers.

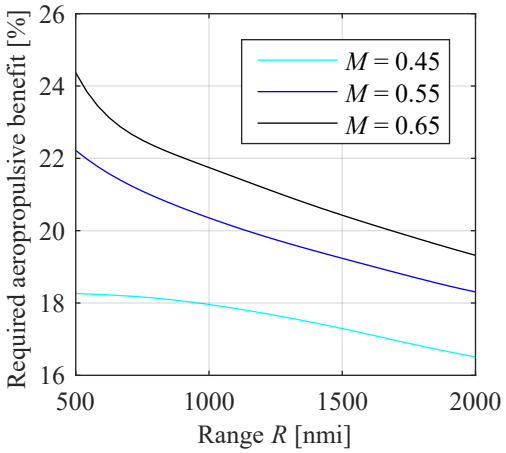

Fig. 7 Influence of Mach number on the aeropropulsive efficiency increase required in order to obtain a 15% increase in PREE (m_{PL} = 15 t, η_{chain} = 0.9, CSP = 3 kW/kg, φ = 0.2).

B. Impact of Electrical-Component Technology Level

This section describes how the aeropropulsive requirements discussed in the previous section evolve as the technology of hybrid-electric powertrain components matures. To this end, Figs. 8 and 9 present the required aeropropulsive benefit for a 15% increase in PREE for missions A and B, respectively, as a function of the electrical drivetrain's chain efficiency and combined specific power. The required aeropropulsive benefit decreases with increasing chain efficiency and CSP, as expected. The trends of Figs. 8 and 9 are similar, although the aeropropulsive requirements are slightly less restrictive for the latter (R = 2000 nmi), as discussed previously. It is interesting to note that these figures also provide information regarding possible trade-offs between the weight and the transmission efficiency of the electrical components. For example, it may be possible to make a more efficient, but heavier, electrical drivetrain, by including active (cryogenic) cooling systems which enable superconductivity on determined components (see e.g. Refs. [11, 43]). Taking the circular marker of Fig. 8b (η_{chain} = 0.9, CSP = 3 kW/kg) as an example, it is evident that a 50% increase in weight of the electrical drivetrain (CSP = 2 kW/kg) is justifiable if it allows the chain efficiency to be increased beyond 95%. Therefore, although evidently a more mature technology will lead to a more competitive turboelectric aircraft, for a given point in time, a trade-off between the chain efficiency and CSP has to be performed to identify the most optimal combination.

Both Fig. 8 and Fig. 9 present the results for three different shaft power ratios, the third of which (φ = 1) corresponds to a fully-turboelectric powertrain. The figures show that higher aeropropulsive benefits are required to compensate higher shaft power ratios: for a fully-turboelectric architecture, the electrical drivetrain has to be able to absorb all the power produced by the gas turbine, leading to very heavy components. Moreover, the higher the shaft power ratio, the higher the amount of power lost in the electrical drivetrain[‡]. Consequently, the aeropropulsive benefits required to offset these penalties and additionally lead to an energy reduction are practically infeasible—even for very advanced technology levels, as indicated in in Figs. 8c and 9c. It appears therefore that a lower shaft power ratio is beneficial. However, the question remains whether the required aeropropulsive benefit is achievable with low shaft power ratios. For example, the required aeropropulsive benefit in Figs. 8a and 9a is of the order of 15%–25%, but this increase in aerodynamic or propulsive efficiency would have to be achieved by means of a smart integration of only 20% of the total shaft power. For some propulsion system layouts this may not constitute a major challenge, if there is a local optimum in

[‡]The power lost in the electrical powertrain branch is $P_{GB} - P_{s2}$ (see Fig. 1), which, by combining Eq. 1, Eq. 4, and $P_{GT} = P_{GB} + P_{s1}$, can be shown to be equal to $\varphi(1-\eta_{chain})(\eta_{chain} + \varphi(1-\eta_{chain}))^{-1} P_{GT}$. Therefore, the losses range from zero, at $\varphi = 0$, to $(1-\eta_{chain})P_{GT}$, at $\varphi = 1$.

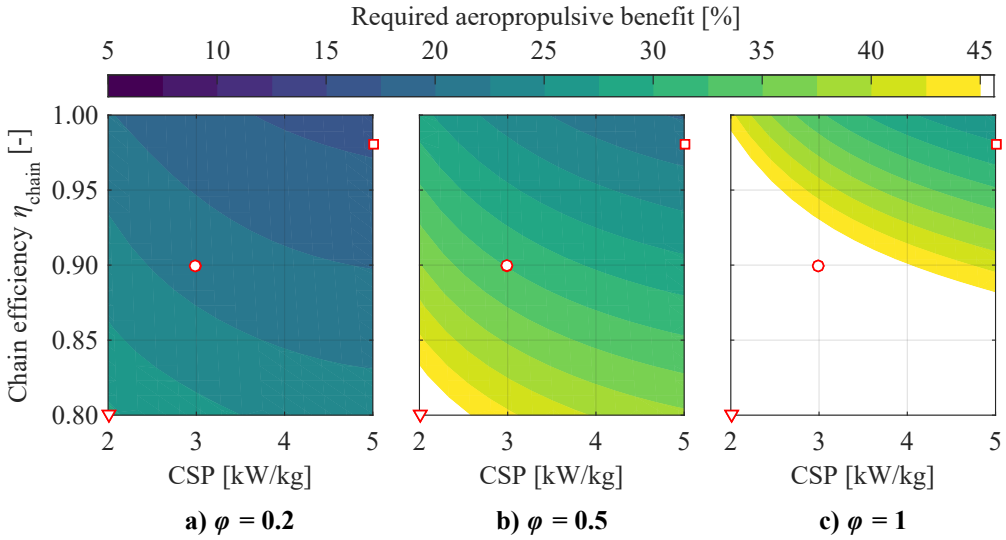

Fig. 8 Aeropropulsive efficiency increase required in order to obtain a 15% increase in PREE for mission A, as a function of the assumed technology level (M = 0.55, m_{PL} = 20 t, R = 650 nmi). Markers indicate the technology scenarios collected in Tables 3 and 4.

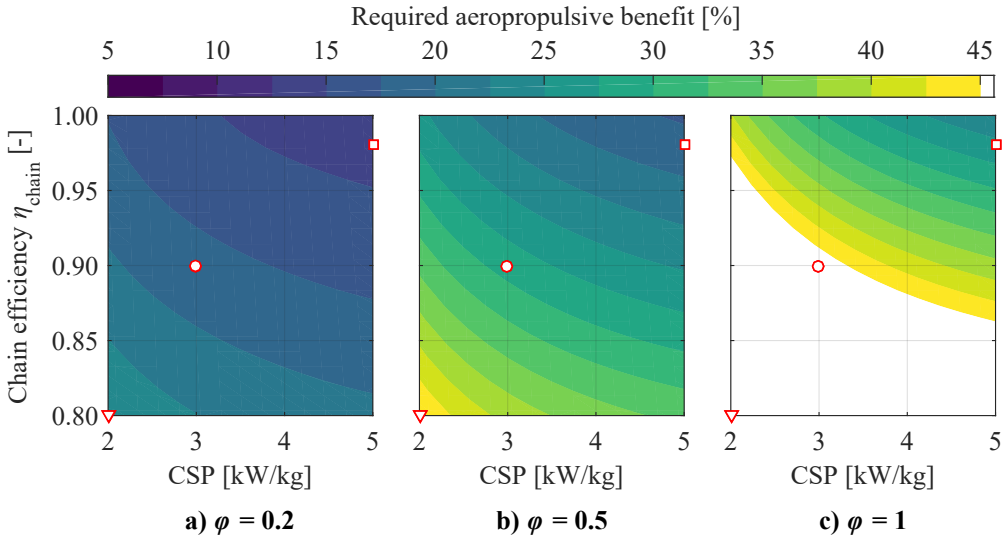

Fig. 9 Aeropropulsive efficiency increase required in order to obtain a 15% increase in PREE for mission B, as a function of the assumed technology level (M = 0.55, m_{PL} = 15 t, R = 2000 nmi). Markers indicate the technology scenarios collected in Tables 3 and 4.

terms of shaft power ratio from an aerodynamic perspective. For example, for a BLI system, the benefit cannot exceed the amount of power dissipated in the fuselage boundary layer, and thus it is only beneficial to divert a fraction of the total shaft power to the fuselage-mounted propulsor (see Fig. 2). However, if, for a determined propulsion-system arrangement, the aeropropulsive benefit grows indefinitely until $\varphi \to 1$, then most likely it will not be possible to take full advantage of the potential of the propulsion system, because of the associated weight penalty. Either way, most of the aeropropulsive efficiency values plotted in Figs. 8 and 9 are difficult, if not impossible, to achieve. This indicates that a 15% reduction in energy consumption is unlikely for the missions considered.

C. Discussion

A summary of the aeropropulsive efficiency requirements is gathered in Tables 3 and 4, for different missions, technology scenarios, and shaft power ratios. As discussed in Sec. II.A, the "mid-term" scenario corresponds to state-of-the-art research goals, which is assumed to be applicable to the 2035-timeframe. The long-term scenario is expected to be applicable only beyond 2050, if ever. However, these timeframes have to be interpreted with caution, since there is no clear forecast. Tables 3 and 4 also categorize the aeropropulsive efficiency requirements into three qualitative groups. Green indicates an aeropropulsive efficiency gain which is considered by the authors to be feasible ($\Delta(\eta_p L/D) \leq 15\%$), though not necessarily easy to achieve. Orange indicates aeropropulsive benefits which are considered extremely difficult to attain ($15\% < \Delta(\eta_p L/D) \leq 25\%$), while the red numbers indicate benefits which are most likely impossible to achieve in practice ($\Delta(\eta_p L/D) > 25\%$). The reader is reminded that the values correspond exclusively to the aeropropulsive benefit enabled by turboelectric propulsion when compared to a conventional gas-turbine based aircraft designed for the same mission and timeframe. The results are shown for a cruise Mach number of $M = 0.55$; results at $M = 0.45$ and $M = 0.65$ can be found in Appendix A.

Table 3 Summary of the aeropropulsive efficiency increase necessary for a 15% increase in PREE with respect to a fuel-based reference aircraft.

			Mission A			Mission B		
		m_{PL} [t]	20			15		
		R [nmi]	650			2000		
		M [-]	0.55			0.55		
Scenario	CSP [kW/kg]	η_{chain} [-]	$\varphi = 0.2$	$\varphi = 0.5$	$\varphi = 1.0$	$\varphi = 0.2$	$\varphi = 0.5$	$\varphi = 1.0$
Near-term	2	0.80	28%	>45%	>45%	25%	>45%	>45%
Mid-term	3	0.90	22%	32%	>45%	19%	29%	>45%
Long-term	5	0.98	17%	21%	28%	14%	19%	26%

Table 4 Summary of the aeropropulsive efficiency increase necessary for a 5% increase in PREE with respect to a fuel-based reference aircraft.

			Mission A			Mission B		
		m_{PL} [t]	20			15		
		R [nmi]	650			2000		
		M [-]	0.55			0.55		
Scenario	CSP [kW/kg]	η_{chain} [-]	$\varphi = 0.2$	$\varphi = 0.5$	$\varphi = 1.0$	$\varphi = 0.2$	$\varphi = 0.5$	$\varphi = 1.0$
Near-term	2	0.80	18%	38%	>45%	17%	37%	>45%
Mid-term	3	0.90	12%	22%	40%	11%	21%	39%
Long-term	5	0.98	8%	12%	18%	7%	11%	18%

Tables 3 and 4 show that, in the near term, a significant reduction in energy consumption by means of turboelectric propulsion is unfeasible. In the mid-term, a 5% reduction in energy consumption is possible if the aeropropulsive efficiency is increased by approximately 11%, although a 15% energy reduction is practically impossible. If the power density and transmission efficiency of the electrical components are further improved, then a 15% reduction in energy consumption may be possible in the long term, provided that the distribution of power leads to a 14%–17% increase in aeropropulsive efficiency. However, these conclusions all consider a shaft power ratio of $\varphi = 0.2$, implying that the aeropropulsive benefit must be gained by distributing around 20% of the total power available. Since the primary powertrain branch (gas turbine and generators) is the dominant contributor to powertrain weight, from an aircraft design perspective, it is generally beneficial to keep it close to the center of gravity. This makes it difficult to reap benefits such

as fuselage boundary-layer ingestion or tip-mounted propulsion with the primary propulsors, and thus a large fraction of the aeropropulsive benefit must be achieved by the smaller, electrically-driven propulsors. Obtaining a 7%–17% benefit in aeropropulsive efficiency is therefore not a trivial target. In any case, Tables 3 and 4 indicate that fully-turboelectric configurations ($\varphi = 1$) are not an effective solution to decrease the energy consumption of transport aircraft.

Although the results show that significant improvements (>5%) in payload-range efficiency by means of turboelectric propulsion are unlikely in the near future, there are still opportunities. For example, the increased power loading enabled by an improvement in low-speed performance can be exploited, especially for aircraft operating from short airfields. Furthermore, a smart integration of the propulsion system may lead to additional benefits which are not captured in this analysis, such as a reduced landing gear size due to increased ground clearance, improved wing bending relief, or a reduced tail size by means of thrust vectoring or differential thrust. Such design considerations must be combined with a smart aerodynamic integration in order to maximize the benefit of hybrid-electric propulsion. Moreover, for a given aeropropulsive benefit, a few percent improvement in PREE can already be gained by flying longer ranges, or by reducing the cruise Mach number to 0.45 (see Tables A.1 and A.2). For such missions, however, other considerations such as flight scheduling and increased crew costs have to be taken into account. Hence, although the results suggest that the turboelectric architecture can be competitive for a high-capacity, long-range turboprop market in terms of vehicular energy consumption, it is unclear whether an expansion of that market would improve the air transportation system as a whole. Given that the medium and long-haul markets are currently responsible for the majority of the environmental footprint of the aviation sector, network-level studies are required which analyze the impact of a reduced flight speed for these markets when hybrid-electric propulsion is included.

IV. Conclusions

A study has been performed with the objective of estimating the aeropropulsive efficiency required from turboelectric aircraft in order to make these configurations more efficient than conventional fuel-based aircraft in terms of energy consumption. To keep the results independent of the specific type of propulsion system employed, a simplified representation of a generic turboelectric aircraft has been assessed in a design-of-experiments, where the preliminary sizing of the aircraft was performed for different mission requirements, technology assumptions, shaft power ratios, and aeropropulsive benefits. The payload-range energy efficiency of the aircraft was then compared to a conventional fuel-based aircraft for the same mission requirements. Both the turboelectric and the reference aircraft were evaluated at their respective optimum cruise altitudes in terms of minimum energy consumption.

The results indicate that both the reference aircraft and the turboelectric variant are most efficient for a harmonic range of approximately 650 nmi, and for payloads above 20 t (200 pax). When comparing the two concepts, the benefit of turboelectric propulsion is found to increase with range, while being practically independent of the payload mass. Moreover, the aeropropulsive benefit required for the turboelectric variant to present a predetermined reduction in energy consumption with respect to the reference aircraft is found to increase with increasing cruise Mach number. Furthermore, the shaft power ratio, φ, is shown to have a large impact on the turboelectric aircraft, with high shaft power ratios ($\varphi \rightarrow 1$) demanding a large increase in aeropropulsive efficiency to offset the weight penalty of the powertrain. This highlights the importance of considering the relation between the achievable aeropropulsive benefit and the shaft power ratio required to achieve it, early in the design process. The results show that, when compared to a conventional, fuel-based aircraft designed for the same timeframe, a 5% reduction in energy consumption is possible in the mid-term (entry into service circa 2035) if an increase in aeropropulsive efficiency of 11% is achieved with a shaft power ratio of 0.2. This aeropropulsive efficiency requirement increases with increasing shaft power ratio, and decreases for higher ranges. The results also suggest that a 15% reduction in energy consumption is only possible with radical improvements in the specific power and transmission efficiency of the electric drivetrain, and if the aeropropulsive efficiency can be increased by 14% using a shaft power ratio of 0.2.

Acknowledgments

This research is part of the European Union's Clean Sky 2 Large Passenger Aircraft program (CS2-LPA-GAM-2014-2015-01). The authors would like to thank Leo Veldhuis (TU Delft), Jos Vankan (NLR), Henk Jentink (NLR), Wim Lammen (NLR), Peter Schmollgruber (Onera), Michael Iwanizki (DLR), Thomas Zill (DLR), and Lars Joergensen (Airbus) for their valuable feedback and contributions to LPA WP 1.6.1.4.

References

[1] Brdnik, A. P., Kamnik, R., Marksel, M., and Božičnik, S., "Market and Technological Perspectives for the New Generation of Regional Passenger Aircraft," *Energies*, Vol. 12(10), 2019, pp. 1–14.

[2] Wroblewski, G. E., and Ansell, P. J., "Mission Analysis and Emissions for Conventional and Hybrid-Electric Commercial Transport Aircraft," 2018 AIAA Aerospace Sciences Meeting, Kissimmee, FL, USA, January 8-12 2018.

[3] Lueckhof, J., and Stumpf, E., "Well-to-Prop - A Holistic Analysis of Emerging Powertrain Concepts for On-Demand Air Mobility Vehicles," 2019 AIAA Aerospace Sciences Meeting, San Diego, CA, USA, January 7-11 2019.

[4] Kreimeier, M., and Stumpf, E., "Benefit evaluation of hybrid electric propulsion concepts for CS-23 aircraft," *CEAS Aeronautical Journal*, Vol. 8, 2017, pp. 691–704.

[5] Kreimeier, M., "Evaluation of On-Demand Air Mobility Concepts with Utilization of Electric Powered Small Aircraft," PhD Dissertation, RWTH Aachen University, Lehrstuhl und Institut für Luft-und Raumfahrtsysteme (ILR), 2018.

[6] Antcliff, K. R., and Capristan, F. M., "Conceptual Design of the Parallel Electric-Gas Architecture with Synergistic Utilization Scheme (PEGASUS) Concept," 17th AIAA/ISSMO Multidisciplinary Analysis and Optimization Conference, Denver, CO, USA, June 5-9 2017.

[7] Strack, M., Chiozzotto, G. P., Iwanizki, M., Plohr, M., and Kuhn, M., "Conceptual Design Assessment of Advanced Hybrid Electric Turboprop Aircraft Configurations," 17th AIAA Aviation Technology, Integration, and Operations Conference, Denver, CO, USA, June 5-9 2017.

[8] Voskuijl, M., van Bogaert, J., and Rao, A. G., "Analysis and design of hybrid electric regional turboprop aircraft," *CEAS Aeronautical Journal*, Vol. 9, 2018, pp. 15–25.

[9] de Vries, R., Hoogreef, M. F. M., and Vos, R., "Preliminary Sizing of a Hybrid-Electric Passenger Aircraft Featuring Over-the-Wing Distributed-Propulsion," 2019 AIAA Aerospace Sciences Meeting, San Diego, CA, USA, January 7-11 2019.

[10] Gologan, C., "Conceptual Design of a STOL Regional-Jet with Hybrid Propulsion System," 26th International Congress of the Aeronautical Sciences, Anchorage, AK, USA, September 14-19 2008.

[11] Jansen, R. H., Bowman, C., Jankovsky, A., Dyson, R., and Felder, J., "Overview of NASA Electrified Aircraft Propulsion Research for Large Subsonic Transports," 53rd AIAA/SAE/ASEE Joint Propulsion Conference, Atlanta, GA, USA, July 10-12 2017. doi:10.2514/6.2017-4701.

[12] Sgueglia, A., Schmollgruber, P., Bartoli, N., Atinault, O., Benard, E., and Morlier, J., "Exploration and Sizing of a Large Passenger Aircraft with Distributed Ducted Electric Fans," 2018 AIAA Aerospace Sciences Meeting, Kissimmee, FL, USA, January 8-12 2018.

[13] Schmollgruber, P., Döll, C., Hermetz, J., Liaboeuf, R., Ridel, M., Cafarelli, I., Atinault, O., François, C., and Paluch, B., "Multidisciplinary Exploration of DRAGON: an ONERA Hybrid Electric Distributed Propulsion Concept," 2019 AIAA Aerospace Sciences Meeting, San Diego, CA, USA, January 7-11 2019.

[14] Ang, A. W. X., Gangoli Rao, A., Kanakis, T., and Lammen, W., "Performance analysis of an electrically assisted propulsion system for a short-range civil aircraft," *Proceedings of the Institution of Mechanical Engineers, Part G: Journal of Aerospace Engineering*, 2018.

[15] Hoogreef, M. F. M., Vos, R., de Vries, R., and Veldhuis, L. L. M., "Conceptual Assessment of Hybrid Electric Aircraft with Distributed Propulsion and Boosted Turbofans," 2019 AIAA Aerospace Sciences Meeting, San Diego, CA, USA, January 7-11 2019.

[16] Isikveren, A. T., Pornet, C., Vratny, P. C., and Schmidt, M., "Optimization of Commercial Aircraft Using Battery-Based Voltaic-Joule/Brayton Propulsion," *Journal of Aircraft*, Vol. 54(1), 2017, pp. 246–261.

[17] Bradley, M. K., and Droney, C. K., "Subsonic Ultra Green Aircraft Research Phase II: N+4 Advanced Concept Development," NASA/CR-2012-217556 Technical Report, 2012.

[18] Felder, J. L., Kim, H. D., and Brown, G. V., "Turboelectric Distributed Propulsion Engine Cycle Analysis for Hybrid-Wing-Body Aircraft," 47th AIAA Aerospace Sciences Meeting, Orlando, FL, USA, January 5-8 2009.

[19] Pornet, C., "Conceptual Design Methods for Sizing and Performance of Hybrid-Electric Transport Aircraft," PhD Dissertation, Technical University of Munich, 2018.

[20] Epstein, A. H., and O'Flarity, S. M., "Considerations for Reducing Aviation's CO_2 with Aircraft Electric Propulsion," *Journal of Propulsion and Power*, Vol. 35(3), 2019, pp. 572–582.

[21] Advisory Council for Aviation Research and Innovation in Europe (ACARE), "Realising Europe's vision for aviation: Strategic research & innovation agenda, Vol. 1," Advisory Council for Aviation Research and Innovation in Europe, 2012.

[22] Bonet, J. T., Schellenger, H. G., Rawdon, B. K., Elmer, K. R., Wakayama, S. R., Brown, D. L., and Guo, Y., "Environmentally Responsible Aviation (ERA) Project - N+2 Advanced Vehicle Concepts Study and Conceptual Design of Subscale Test Vehicle (STV): Final Report," Technical Report NASA/CR-2011-216519, December 2011.

[23] de Vries, R., Brown, M., and Vos, R., "Preliminary Sizing Method for Hybrid-Electric Distributed-Propulsion Aircraft," *Journal of Aircraft*, 2019.

[24] National Academies of Sciences, Engineering, and Medicine, *Commercial Aircraft Propulsion and Energy Systems Research: Reducing Global Carbon Emissions*, National Academies Press, 2016.

[25] Brelje, B. J., and Martins, J. R. R. A., "Electric, hybrid, and turboelectric fixed-wing aircraft: A review of concepts, models, and design approaches," *Progress in Aerospace Sciences*, Vol. 104, 2019, pp. 1–19.

[26] Gladin, J. C., Trawick, D., Mavris, D., Armstrong, M., Bevis, D., and Klein, K., "Fundamentals of Parallel Hybrid Turbofan Mission Analysis with Application to the Electrically Variable Engine," 2018 AIAA/IEEE Electric Aircraft Technologies Symposium, Cincinnati, OH, USA, July 9-11 2018.

[27] Lents, C., Hardin, L., Rheaume, J., and Kohlman, L., "Parallel Hybrid Gas-Electric Geared Turbofan Engine Conceptual Design and Benefits Analysis," 52nd AIAA/SAE/ASEE Joint Propulsion Conference, Salt Lake City, UT, USA, July 25-27 2016.

[28] Seitz, A., Nickl, M., Stroh, A., and Vratny, P. C., "Conceptual study of a mechanically integrated parallel hybrid electric turbofan," *Proceedings of the Institution of Mechanical Engineers, Part G: Journal of Aerospace Engineering*, 2018.

[29] Spierling, T., and Lents, C., "Parallel Hybrid Propulsion System for a Regional Turboprop: Conceptual Design and Benefits Analysis," AIAA Propulsion and Energy 2019 Forum, Indianapolis, IN, USA, August 19-22 2019.

[30] Schiltgen, B., Freeman, J. L., and Hall, D. W., "Aeropropulsive Interaction and Thermal System Integration within the ECO-150: A Turboelectric Distributed Propulsion Airliner with Conventional Electric Machines," 16th AIAA Aviation Technology, Integration and Operations Conference, Washington, DC, USA, June 13-17 2016.

[31] Hoogreef, M. F. M., de Vries, R., Sinnige, T., and Vos, R., "Synthesis of Aero-Propulsive Interaction Studies applied to Conceptual Hybrid-Electric Aircraft Design," 2020 AIAA Aerospace Sciences Meeting, Orlando, FL, USA, January 6-10 2020.

[32] Patterson, M. D., "Conceptual Design of High-Lift Propeller Systems for Small Electric Aircraft," PhD Dissertation, Georgia Institute of Technology, 2016.

[33] Marcus, E. A. P., de Vries, R., Raju Kulkarni, A., and Veldhuis, L. L. M., "Aerodynamic Investigation of an Over-the-Wing Propeller for Distributed Propulsion," 2018 AIAA Aerospace Sciences Meeting, Kissimmee, FL, USA, January 8-12 2018.

[34] Bijewitz, J., Seitz, A., Hornung, M., and Isikveren, A. T., "Progress in Optimizing the Propulsive Fuselage Aircraft Concept," *Journal of Aircraft*, Vol. 54(5), 2017, pp. 1979–1989.

[35] Sinnige, T., van Arnhem, N., Stokkermans, T. C. A., Eitelberg, G., and Veldhuis, L. L. M., "Wingtip-Mounted Propellers: Aerodynamic Analysis of Interaction Effects and Comparison with Conventional Layout," *Journal of Aircraft*, Vol. 56(1), 2019, pp. 295–312.

[36] Bijewitz, J., Seitz, A., and Hornung, M., "A review of recent aircraft concepts employing synergistic propulsion-airframe integration," 30th Congress of the International Council of the Aeronautical Sciences, Daejeon, Korea, September 25-30 2016.

[37] Jansen, R. H., Brown, G. V., Felder, J. L., and Duffy, K. P., "Turboelectric Aircraft Drive Key Performance Parameters and Functional Requirements," 51st AIAA/SAE/ASEE Joint Propulsion Conference, Orlando, FL, USA, July 27-29 2015.

[38] Borer, N. K., Patterson, M. D., Viken, J. K., Moore, M. D., Clarke, S., Redifer, M. E., Christie, R. J., Stoll, A. M., Dubois, A., Bevirt, J. B., Gibson, A. R., Foster, T. J., and Osterkamp, P. G., "Design and Performance of the NASA SCEPTOR Distributed Electric Propulsion Flight Demonstrator," 16th AIAA Aviation Technology, Integration, and Operations Conference, Washington, DC, USA, June 13-17 2016.

[39] Smith Jr., L. H., "Wake Ingestion Propulsion Benefit," *Journal of Propulsion and Power*, Vol. 9(1), 1993, pp. 74–83.

[40] Torenbeek, E., *Optimum Cruise Performance of Subsonic Transport Aircraft*, Delft University Press, 1998.

[41] Finger, D. F., de Vries, R., Vos, R., Braun, C., and Bil, C., "A Comparison of Hybrid-Electric Aircraft Sizing Methods," 2020 AIAA Aerospace Sciences Meeting, Orlando, FL, USA, January 6-10 2020.

[42] Nicolosi, F., Corcione, S., Trifari, V., Cusati, V., Ruocco, M., and Della Vecchia, P., "Performance Evaluation and DOC Estimation of an Innovative Turboprop Configuration," 2018 Aviation Technology, Integration, and Operations Conference, Atlanta, GA, USA, June 25-29 2018.

[43] Luongo, C. A., Masson, P. J., Nam, T., Mavris, D., Kim, H. D., Brown, G. V., Waters, M., and Hall, D., "Next Generation More-Electric Aircraft: A Potential Application for HTS Superconductors," *IEEE Transactions on Applied Superconductivity*, Vol. 19(3), 2009, pp. 1055–1068.

Appendix A: Aeropropulsive Efficiency Requirements at $M = 0.45$ and $M = 0.65$.

Table A.1 Aeropropulsive efficiency increase necessary for a 15% increase in PREE with respect to a fuel-based reference aircraft, for a cruise Mach number of $M = 0.45$.

			Mission A			Mission B		
		m_{PL} [t]	20			15		
		R [nmi]	650			2000		
		M [-]	0.45			0.45		
Scenario	CSP [kW/kg]	η_{chain} [-]	$\varphi = 0.2$	$\varphi = 0.5$	$\varphi = 1.0$	$\varphi = 0.2$	$\varphi = 0.5$	$\varphi = 1.0$
Near-term	2	0.80	24%	>45%	>45%	23%	44%	>45%
Mid-term	3	0.90	18%	28%	>45%	17%	27%	>45%
Long-term	5	0.98	15%	18%	24%	13%	17%	23%

Table A.2 Aeropropulsive efficiency increase necessary for a 5% increase in PREE with respect to a fuel-based reference aircraft, for a cruise Mach number of $M = 0.45$.

			Mission A			Mission B		
		m_{PL} [t]	20			15		
		R [nmi]	650			2000		
		M [-]	0.45			0.45		
Scenario	CSP [kW/kg]	η_{chain} [-]	$\varphi = 0.2$	$\varphi = 0.5$	$\varphi = 1.0$	$\varphi = 0.2$	$\varphi = 0.5$	$\varphi = 1.0$
Near-term	2	0.80	15%	34%	>45%	15%	34%	>45%
Mid-term	3	0.90	10%	18%	36%	9%	18%	37%
Long-term	5	0.98	6%	9%	15%	6%	9%	15%

Table A.3 Aeropropulsive efficiency increase necessary for a 15% increase in PREE with respect to a fuel-based reference aircraft, for a cruise Mach number of $M = 0.65$.

			Mission A			Mission B		
		m_{PL} [t]	20			15		
		R [nmi]	650			2000		
		M [-]	0.65			0.65		
Scenario	CSP [kW/kg]	η_{chain} [-]	$\varphi = 0.2$	$\varphi = 0.5$	$\varphi = 1.0$	$\varphi = 0.2$	$\varphi = 0.5$	$\varphi = 1.0$
Near-term	2	0.80	32%	>45%	>45%	27%	>45%	>45%
Mid-term	3	0.90	23%	37%	>45%	20%	33%	>45%
Long-term	5	0.98	18%	24%	33%	15%	20%	30%

Table A.4 Aeropropulsive efficiency increase necessary for a 5% increase in PREE with respect to a fuel-based reference aircraft, for a cruise Mach number of $M = 0.65$.

			Mission A			Mission B		
		m_{PL} [t]	20			15		
		R [nmi]	650			2000		
		M [-]	0.65			0.65		
Scenario	CSP [kW/kg]	η_{chain} [-]	$\varphi = 0.2$	$\varphi = 0.5$	$\varphi = 1.0$	$\varphi = 0.2$	$\varphi = 0.5$	$\varphi = 1.0$
Near-term	2	0.80	22%	>45%	>45%	20%	44%	>45%
Mid-term	3	0.90	13%	27%	>45%	12%	25%	>45%
Long-term	5	0.98	8%	14%	24%	8%	13%	22%